C. R. Mecanique 345 (2017) 764–778

Contents lists available at ScienceDirect

Comptes Rendus Mecanique

www.sciencedirect.com

Effect of regularized functions on the dynamic response of a clutch system using a high-order algorithm

Youssef Hilali, Bouazza Braikat *, Hassane Lahmam, Noureddine Damil

Laboratoire d'ingénierie et matériaux (LIMAT), Faculté des sciences Ben M'Sik, Université Hassan-II de Casablanca, Sidi Othman, B.P. 7955, Casablanca, Morocco

ARTICLE INFO

Article history:
Received 29 May 2017
Accepted 12 August 2017
Available online 18 September 2017

Keywords:
Clutch
Nonlinear dynamics
No smoothed functions
Regularization technique
High-order approach
Homotopy transformation
Taylor series

ABSTRACT

The main objective of this work is to propose some regularization techniques for modeling contact actions in a clutch system and to solve the obtained nonlinear dynamic problem by a high-order algorithm. This device is modeled by a discrete mechanical system with eleven degrees of freedom. In several works, the discontinuous models of the contact actions are replaced by the smoothed functions using the hyperbolic tangent. We propose, in this work, to replace the discontinuous model by a regularized model with new continuous functions that permit us to search the solution under Taylor series expansion. This regularized model approaches better the discontinuous model than the model based on the smoothing functions, especially in the vicinity of the zone of singularities. To solve the equations of motion of discrete mechanical systems, we propose to use a high-order algorithm combining a time discretization, a change of variable based on the previous time, a homotopy transformation and Taylor series expansion in the continuation process. The results obtained by this modeling are compared with those computed by the Newton–Raphson algorithm.

1. Introduction

In contrast to gears, which are considered to be motion transmission elements by obstacles, the clutch is a complex mechanism commonly used in motors, for transmitting the motion by means of a high friction effect between adjacent disks. The clutch plays an important role, not just in the commitment and the separation between the motor and the gearbox, but also in the prevention of the damage of the box speed and the vibration reduction of the rest of the vehicle when there is a modification in the rotation frequency of the disk. During the past years, several studies [1–7] have been developed to describe the nonlinear dynamic behavior of the clutch system in order to study the effect of different key parameters that affect its movement. In many studies, the clutch is modeled by a discrete mechanical system composed of torsional and linear elastic springs of negligible mass and of damping elements and disks assumed to be rigid.

Walha et al. [7] have studied a defective clutch modeled by a mechanical system with eleven degrees of freedom by introducing nonlinearities of the dry friction, a two-stage stiffness, and a spline clearance in order to analyze the effect of defects in angular misalignment and in parallelism on movement. Recently, Walha et al. [8] have proposed a new two-stage

* Corresponding author.
E-mail address: b.braikat@gmail.com (B. Braikat).

http://dx.doi.org/10.1016/j.crme.2017.08.002
1631-0721/

model involving a helical-gear clutch system with twenty-seven degrees of freedom. The differential equations are solved numerically by the Runge–Kutta integration scheme [9] using smoothing by the hyperbolic tangent function. Thus, they have showed that the eccentricity defect affects the nonlinear dynamic behavior of the studied mechanism.

The assembly of different technical components in the clutch system leads to localized contact nonlinearities and important couplings. These nonlinearities are often modeled by piecewise linear functions. To overcome the difficulty of the discontinuity in the numerical integration, some researchers have used a linearization technique that consists in transforming the nonlinear problem into linear problems. But most authors [3,7,10–13] have used the smoothing procedure for the treatment of contact actions.

Kim et al. [14] have proposed four ways of smoothing discontinuous functions using the hyperbolic tangent and arc-tangent functions that provide a good approximation with respect to the hyperbolic-cosine function and the quintic spline. They have proved it by studying the influence of the smoothing factor on the frequency response of a system that contains a clearance nonlinearity. Works by Driss et al. [6,15] and Walha et al. [7] are based on the use of the hyperbolic tangent function to smooth three types of singular functions of a torsional model. Duan et al. [12] have investigated the dynamics of a mechanical oscillator with a pre-load nonlinearity by the multi-harmonic method using the arc-tangent function for smoothing the non-analytical relationship. Duan et al. [3] have used the hyperbolic tangent function to approximate the classical function of Coulomb friction.

According to Duan et al. [10], the value of the conditioning factor should be carefully selected to ensure the appropriate representation of the discontinuous function. The increase in the value of the smoothing factor improves the approximation of the discontinuous models. However, a larger value of this parameter can lead to numerical instabilities that generate a considerable computation time [3]. In another work [13], it has been shown that, for small values of this parameter, the convergence is fast, but it is not preferred, since it induces a bad approximation and therefore the calculated response may not be sufficiently precise.

In this work, we are interested in the numerical simulation of nonlinear dynamics of a clutch system using a new version of a high-order algorithm [16–20] with a new modeling of the different contact actions. Our numerical algorithm is essentially based on the discrete model proposed in the article [15], which represents the clutch mechanism by a spring-mass-damper system, and whose equations of motion are solved using the numerical integration scheme of Runge–Kutta. In our modeling, we propose a new improved version of the modeling of different contact actions in a clutch mechanism existing in the literature in order to achieve a good approximation, and we try to obtain a realistic response. To show the effectiveness of the numerical approach to simulate the nonlinear dynamic response of the considered mechanical system, we have chosen as a reference the Newton–Raphson algorithm [21] coupled with the Newmark integration scheme with the use of the hyperbolic tangent function, and we used thereafter the regularization developed in this work. The high-order approach is used for the purpose of reducing the computation time. This approach, allowing the construction of the curve solution branch by branch, is based on coupling power series expansion and on a continuation process. In our analysis, we study the effect of different regularization parameters on the nonlinear dynamic responses of the considered clutch system.

2. Dynamic model of the clutch mechanism

The clutch mechanism is modeled by a physical system shown in Fig. 1. This system is comprised of two blocks. The first contains the flywheel and the cover (m_1, I_1), the diaphragm spring and the pressing plate (m_2, I_2), while the second is comprised of the friction shoes (m_3, I_3), the hub of the clutch (m_4, I_4) and the rest of the transmission (m_5, I_5), with I_i and m_i being respectively the mass and the torsional inertia of the ith element of the clutch. Each block is supported by a flexible bearing of bending rigidity k_{z_i} and of traction–compression stiffness k_{x_i} and k_{y_i}. This bearing is connected in parallel with the damping elements c_{x_i}, c_{y_i} and c_{z_i}, where i is the number of blocks $(i = 1, 2)$. The contact between the two blocks is performed by the torques and the friction forces. The friction torque $T_f(\dot{\delta}_2)$ represents the torsional friction between the pressing plate and friction shoes and $T_f(\dot{\delta}_3)$ represents the friction torque between the flywheel and the friction shoes. In both cases, the movement of these blocks, in the plan xy, induces tangential friction forces $F_{T_{x_{1/2}}}$ and $F_{T_{y_{1/2}}}$ that express the actions applied by the first block on the second in both directions x and y, respectively. The action of the spring diaphragm, which allows the components of the first block to turn at the same angular speed as those of the second block, is modeled by a torsional spring of stiffness k_d and a negligible mass. The cover applies a pressure P to maintain both the flywheel, pressing plate, and friction shoes in permanent contact to ensure a perfect transmission. The actions of the torsion springs which bind the splined hub with friction shoes are represented by the term $K_{dss} f_{dss}(\delta_i)$, with K_{dss} being the equivalent stiffness of the equivalent linear spring and $f_{dss}(\delta_i)$ is the contact force. The backlash space in the splined attachment between the hub and the output shaft can be defined by the term $K_{sc} f_{sc}(\delta_i)$, where K_{sc} represents the torsional stiffness of the shaft and $f_{sc}(\delta_i)$ is the function that models the loss of contact. The equation of motion of this discrete model verified by the vector of generalized coordinates can be written in the following matrix form:

$$\begin{aligned}[M]\{\ddot{q}\} + [C]\{\dot{q}\} \; + \; [K]\{q\} + f_{dss}(\delta_4)\{\varphi_{dss}\} + f_{sc}(\delta_5)\{\varphi_{sc}\} + T_f(\dot{\delta}_2)\{\varphi_2\} \\ + \; T_f(\dot{\delta}_3)\{\varphi_3\} + F_{T_{x_{1/2}}}\{\varphi_{T_x}\} + F_{T_{y_{1/2}}}\{\varphi_{T_y}\} = \{F_{ext}(t)\}\end{aligned} \tag{1}$$

where $[M]$ represents the mass matrix given by:

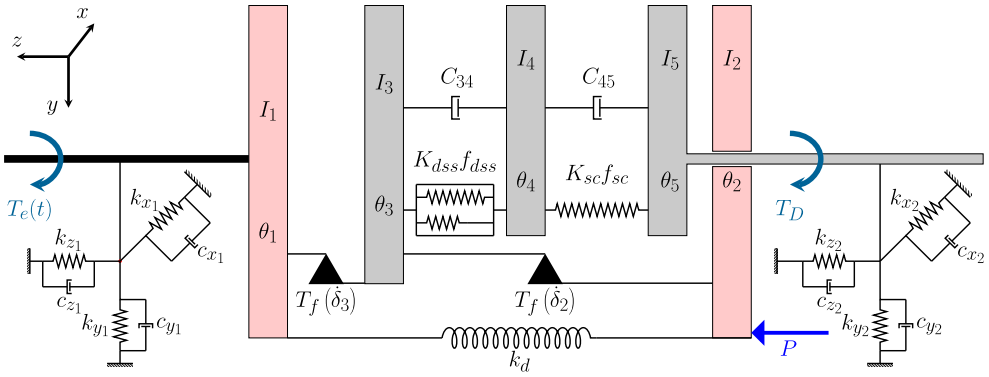

Fig. 1. Modeling of the clutch system with a discrete mechanical system taking into account of the different types of contact.

$$[M] = \begin{bmatrix} M_1 & 0 & 0 & 0 & 0 & 0 & 0 & 0 & 0 & 0 & 0 \\ 0 & M_1 & 0 & 0 & 0 & 0 & 0 & 0 & 0 & 0 & 0 \\ 0 & 0 & M_1 & 0 & 0 & 0 & 0 & 0 & 0 & 0 & 0 \\ 0 & 0 & 0 & M_2 & 0 & 0 & 0 & 0 & 0 & 0 & 0 \\ 0 & 0 & 0 & 0 & M_2 & 0 & 0 & 0 & 0 & 0 & 0 \\ 0 & 0 & 0 & 0 & 0 & M_2 & 0 & 0 & 0 & 0 & 0 \\ 0 & 0 & 0 & 0 & 0 & 0 & I_1+I_2 & 0 & 0 & 0 & 0 \\ 0 & 0 & 0 & 0 & 0 & 0 & 0 & I_2+I_3 & 0 & 0 & 0 \\ 0 & 0 & 0 & 0 & 0 & 0 & 0 & 0 & I_1+I_3 & 0 & 0 \\ 0 & 0 & 0 & 0 & 0 & 0 & 0 & 0 & 0 & I_3+I_4 & 0 \\ 0 & 0 & 0 & 0 & 0 & 0 & 0 & 0 & 0 & 0 & I_4+I_5 \end{bmatrix} \tag{2}$$

with $M_1 = m_1 + m_2$ and $M_2 = m_3 + m_4 + m_5$ represent the masses of the two blocks, $[C]$ is the damping matrix given by:

$$[C] = \begin{bmatrix} c_{x_1} & 0 & 0 & 0 & 0 & 0 & 0 & 0 & 0 & 0 & 0 \\ 0 & c_{y_1} & 0 & 0 & 0 & 0 & 0 & 0 & 0 & 0 & 0 \\ 0 & 0 & c_{z_1} & 0 & 0 & 0 & 0 & 0 & 0 & 0 & 0 \\ 0 & 0 & 0 & c_{x_2} & 0 & 0 & 0 & 0 & 0 & 0 & 0 \\ 0 & 0 & 0 & 0 & c_{y_2} & 0 & 0 & 0 & 0 & 0 & 0 \\ 0 & 0 & 0 & 0 & 0 & c_{z_2} & 0 & 0 & 0 & 0 & 0 \\ 0 & 0 & 0 & 0 & 0 & 0 & 0 & 0 & 0 & 0 & 0 \\ 0 & 0 & 0 & 0 & 0 & 0 & 0 & 0 & 0 & -c_{34} & 0 \\ 0 & 0 & 0 & 0 & 0 & 0 & 0 & 0 & 0 & -c_{34} & 0 \\ 0 & 0 & 0 & 0 & 0 & 0 & 0 & 0 & 0 & 2c_{34} & -c_{45} \\ 0 & 0 & 0 & 0 & 0 & 0 & 0 & 0 & 0 & -c_{34} & 2c_{45} \end{bmatrix} \tag{3}$$

condition contact actions with c_{34} and c_{45} are the torsional viscous damping coefficients, c_{x_i}, c_{y_i} and c_{z_i} are the linear damping coefficients, $[K]$ is the stiffness matrix of the discrete model defined by:

$$[K] = \begin{bmatrix} k_{x_1} & 0 & 0 & 0 & 0 & 0 & 0 & 0 & 0 & 0 & 0 \\ 0 & k_{y_1} & 0 & 0 & 0 & 0 & 0 & 0 & 0 & 0 & 0 \\ 0 & 0 & k_{z_1} & 0 & 0 & 0 & 0 & 0 & 0 & 0 & 0 \\ 0 & 0 & 0 & k_{x_2} & 0 & 0 & 0 & 0 & 0 & 0 & 0 \\ 0 & 0 & 0 & 0 & k_{y_2} & 0 & 0 & 0 & 0 & 0 & 0 \\ 0 & 0 & 0 & 0 & 0 & k_{z_2} & 0 & 0 & 0 & 0 & 0 \\ 0 & 0 & 0 & 0 & 0 & 0 & 2k_{\mathrm{d}} & 0 & 0 & 0 & 0 \\ 0 & 0 & 0 & 0 & 0 & 0 & -k_{\mathrm{d}} & 0 & 0 & 0 & 0 \\ 0 & 0 & 0 & 0 & 0 & 0 & k_{\mathrm{d}} & 0 & 0 & 0 & 0 \\ 0 & 0 & 0 & 0 & 0 & 0 & 0 & 0 & 0 & 0 & 0 \\ 0 & 0 & 0 & 0 & 0 & 0 & 0 & 0 & 0 & 0 & 0 \end{bmatrix} \tag{4}$$

$\{F_{\mathrm{ext}}(t)\}$ is the vector of external forces dependent on time, which is given by:

$$^{\mathrm{t}}\{F_{\mathrm{ext}}(t)\} = < 0, 0, P, 0, 0, 0, T_{\mathrm{e}}(t), 0, T_{\mathrm{e}}(t), 0, T_D > \tag{5}$$

with $T_{\mathrm{e}}(t)$ is an input torque applied by an asynchronous motor which is composed of mean T_{m} and pulsating $T_{\mathrm{p}}(t)$ components. This input torque is given under the form of Fourier series expansion by:

$$T_e(t) = T_m + T_p(t) = T_m + \sum_{n=1}^{n_{max}} T_{pn} \cos\left(\omega_{pn} t + \phi_{pn}\right) \tag{6}$$

with $\omega_{pn} = nN_e f_e$, N_e is the number of engine cylinders [22,23], ϕ_{pn} is the associated phase lag [14]; n_{max} is the harmonic order of the firing sequence, T_{pn} is the amplitude for the nth harmonic and f_e is the frequency excitation. In this paper, only the fundamental term ($n_{max} = 1$) is considered for the sake of simplicity and the phase angle assumed to be zero. T_D is the resisting torque applied by the rest of driveling system assumed equal to the average component of the motor torque T_m. The independent temporal vectors $\{\varphi_{dss}\}$, $\{\varphi_{sc}\}$, $\{\varphi_2\}$, $\{\varphi_3\}$, $\{\varphi_{T_x}\}$ and $\{\varphi_{T_y}\}$ are expressed by:

$$\begin{cases} {}^t\{\varphi_{dss}\} &= <0,0,0,0,0,0,0,-K_{dss},-K_{dss},2K_{dss},-K_{dss}> \\ {}^t\{\varphi_{sc}\} &= <0,0,0,0,0,0,0,0,0,-K_{sc},2K_{sc}> \\ {}^t\{\varphi_2\} &= <0,0,0,0,0,0,0,-1,2,1,-1,0> \\ {}^t\{\varphi_3\} &= <0,0,0,0,0,0,0,1,1,2,-1,0> \\ {}^t\{\varphi_{T_x}\} &= <-2,0,0,2,0,0,0,0,0,0,0,0> \\ {}^t\{\varphi_{T_y}\} &= <2,0,0,-2,0,0,0,0,0,0,0,0> \end{cases} \tag{7}$$

The vector of the generalized coordinates $\{q\}$ contains eleven degrees of freedom and it is given by:

$${}^t\{q\} = < x_1, y_1, z_1, x_2, y_2, z_2, \delta_1, \delta_2, \delta_3, \delta_4, \delta_5 > \tag{8}$$

with x_i, y_i and z_i are the linear displacements of bearings in the three directions x, y and z, δ_i $(i = 1, .., 5)$ are the relative angular displacements defined by $\delta_1 = \theta_1 - \theta_2$, $\delta_2 = \theta_2 - \theta_3$, $\delta_3 = \theta_1 - \theta_3$, $\delta_4 = \theta_3 - \theta_4$, and $\delta_5 = \theta_4 - \theta_5$, θ_i $(i = 1, ..., 5)$ are the absolute rotation angles of the different elements. The quantities $\{\dot{q}\}$ and $\{\ddot{q}\}$ denote the velocity and acceleration vectors, respectively.

3. Mathematical modeling of contact actions

3.1. Modeling of friction contacts

In many transmission mechanisms, the contact is carried out by friction between surfaces. Previous studies [5,24,25] have used the friction torque function of the classical Coulomb model $T_f(\dot{\delta}_i)$, which depends on the relative velocity $\dot{\delta}_i$ $(i = 2, 3)$ between the contact surfaces and is expressed as:

$$T_f(\dot{\delta}_i) = \begin{cases} T_s & \text{if} \quad \dot{\delta}_i > 0 \\ [-T_s \quad T_s] & \text{if} \quad \dot{\delta}_i = 0 \\ -T_s & \text{if} \quad \dot{\delta}_i < 0 \end{cases} \quad , \quad i = 2, 3 \tag{9}$$

where T_s is the saturation of the friction torque. This model is an ideal case characterized by the abrupt change in the friction torque between sticking and sliding. It is considered the simplest [26], defining three states of contact: positive sliding, negative sliding, and pure collage [27].

The tangential frictions of the stock $F_{T_{x_{1/2}}}$ and $F_{T_{y_{1/2}}}$ due to the translation in both directions x and y, respectively, are represented by Coulomb's theorem [6,7,15] and given by:

$$\begin{cases} F_{T_{x_{1/2}}} = -\mu_k P \frac{\dot{\delta}_{Tx}}{\|\dot{\delta}_{Tx}\|} \quad , \quad \dot{\delta}_{T_x} = \dot{x}_2 - \dot{x}_1 \quad , \quad \frac{\dot{\delta}_{Tx}}{\|\dot{\delta}_{Tx}\|} \cong \operatorname{sgn}(\dot{x}_2 - \dot{x}_1) \\ F_{T_{y_{1/2}}} = -\mu_k P \frac{\dot{\delta}_{Ty}}{\|\dot{\delta}_{Ty}\|} \quad , \quad \dot{\delta}_{T_y} = \dot{y}_2 - \dot{y}_1 \quad , \quad \frac{\dot{\delta}_{Ty}}{\|\dot{\delta}_{Ty}\|} \cong \operatorname{sgn}(\dot{y}_2 - \dot{y}_1) \end{cases} \tag{10}$$

where sgn is the conventional triple-valued signum function, $\dot{\delta}_{T_x}$ and $\dot{\delta}_{T_y}$ are the relative velocities in the directions x and y and μ_k is the kinetic friction coefficient.

3.2. Modeling of the progression springs

The springs in the clutch disk are called torsion damper springs. Their main function is to absorb the fluctuations of the engine revolutions. These springs absorb the shock of clutch engagement during the acceleration. During the braking of the motor, the springs are compressed to reduce the deceleration shock. The alternative change of engagement of one or two springs into action can be described by three piecewise linear regimes defining the function $f_{DSS}(\delta_4)$ can be written as [23,28]:

$$f_{\mathrm{dss}}(\delta_4) = \begin{cases} \delta_4 - (1-\alpha_{\mathrm{dss}})b_{\mathrm{dss}} & \text{if} \quad \delta_4 > b_{\mathrm{dss}} \\ \alpha_{\mathrm{dss}}\delta_4 & \text{if} \quad -b_{\mathrm{dss}} \le \delta_4 \le b_{\mathrm{dss}} \\ \delta_4 + (1-\alpha_{\mathrm{dss}})b_{\mathrm{dss}} & \text{if} \quad \delta_4 < -b_{\mathrm{dss}} \end{cases} \tag{11}$$

where b_{dss} is the value of half of the gap space between the two springs and α_{dss} is the stiffness ratio between the two contact states of the piecewise-linear elastic function that satisfies the condition $0 < \alpha_{\mathrm{dss}} \le 1$.

3.3. Contact modeling in the splined hub

It is well known that the contact between the splined shaft and the coupling hub requires an inevitable clearance. It is defined as the excess space whose value must not be excessive for the operating requirements. For this, it must be fixed carefully to respect the typical tolerances of the manufacturing and of the operation. This backlash space in the splined attachment induces minor movements between the output shaft and the hub. This undesirable behavior is represented mathematically by the function $f_{\mathrm{sc}}(\delta_5)$ and described by the following equation [6–8,15]:

$$f_{\mathrm{sc}}(\delta_5) = \begin{cases} \delta_5 - b_{\mathrm{sc}} & \text{if} \quad \delta_5 > b_{\mathrm{sc}} \\ 0 & \text{if} \quad -b_{\mathrm{sc}} \le \delta_5 \le b_{\mathrm{sc}} \\ \delta_5 + b_{\mathrm{sc}} & \text{if} \quad \delta_5 < -b_{\mathrm{sc}} \end{cases} \tag{12}$$

where b_{sc} represents the half of the spline clearance.

4. Regularization technique of the various contact actions

In this section, we recall the various smoothing functions existing in the literature, which model the different contact actions in the studied mechanism and we give the steps leading to the regularization of these actions according to our modeling [29]. In the works [3,7,10–13], the authors have used a smoothing technique based on the hyperbolic tangent function. The reason to use the regularizing technique in this work is, on the one hand, the applicability of the technique of Taylor series expansions [30,31] and, on the other hand, the improvement of the approximations existing especially in the vicinity of the singularity points.

In order to explain our regularization technique, let us consider the non-regularized law (11) that models the progression springs stiffness. This law has been used by several authors [6,8,14,15] in a smooth shape using the hyperbolic tangent function defined as follows:

$$\begin{aligned} \bar{f}_{\mathrm{dss}}(\delta_4) \;=\; & \delta_4 + \tfrac{(1-\alpha_{\mathrm{dss}})}{2}((\delta_4 - b_{\mathrm{dss}})\tanh(\sigma_{\mathrm{dss}}(\delta_4 - b_{\mathrm{dss}})) \\ & - (\delta_4 + b_{\mathrm{dss}})\tanh(\sigma_{\mathrm{dss}}(\delta_4 + b_{\mathrm{dss}}))) \end{aligned} \tag{13}$$

where σ_{dss} is the smoothing parameter. In this paper, we propose to replace the non-regularized double stage stiffness function $\bar{f}_{\mathrm{dss}}(\delta_4)$ of (13) by the following regularized function given by:

$$\tilde{f}_{\mathrm{dss}}(\delta_4) = \delta_4 + \frac{1}{2}(h_{\mathrm{dss}}(\delta_4) - g_{\mathrm{dss}}(\delta_4)) \tag{14}$$

where $h_{\mathrm{dss}}(\delta_4)$ and $g_{\mathrm{dss}}(\delta_4)$ are square root of a polynomial function given by:

$$\begin{aligned} h_{\mathrm{dss}}(\delta_4) \;&=\; \sqrt{((1-\alpha_{\mathrm{dss}})(\delta_4 - b_{\mathrm{dss}}))^2 + 4\eta_{\mathrm{dss}}^2 b_{\mathrm{dss}}^2} \\ g_{\mathrm{dss}}(\delta_4) \;&=\; \sqrt{((1-\alpha_{\mathrm{dss}})(\delta_4 + b_{\mathrm{dss}}))^2 + 4\eta_{\mathrm{dss}}^2 b_{\mathrm{dss}}^2} \end{aligned} \tag{15}$$

where η_{dss} is the regularized parameter. In Fig. 2, we represent the influence of different smoothing and regularization parameters on the quality of the approximation. According to Figs. 2a and 2b, one can conclude that the proposed regularization, in this work, approximates perfectly the singularity zones when the used parameter is small. Indeed, the curve of the regularized law fits better with the shape of the singularity of equation (11).

Similarly, to regularize the law modeling the actions in the clearance of splines (12), it suffices to take $\alpha_{\mathrm{dss}} = 0$ in the previous regularization. Then, we obtain the following regularized law:

$$\tilde{f}_{\mathrm{sc}}(\delta_5) = \delta_5 + \frac{1}{2}(h_{\mathrm{sc}}(\delta_5) - g_{\mathrm{sc}}(\delta_5)) \tag{16}$$

where $h_{\mathrm{sc}}(\delta_5)$ and $g_{\mathrm{sc}}(\delta_5)$ are given by:

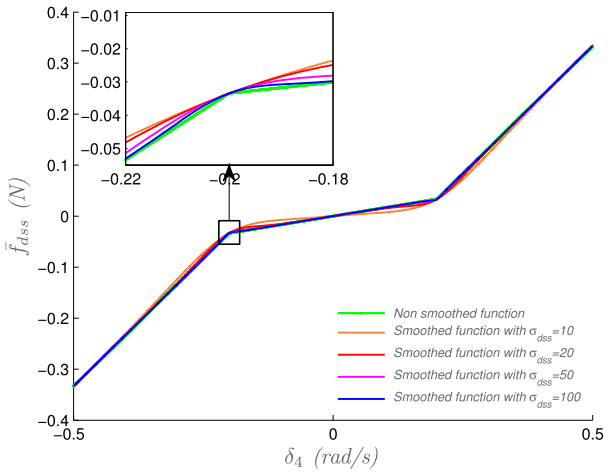

(a) Smoothing technique for the values $\sigma_{\mathrm{dss}} = 10, 20, 50, 100$.

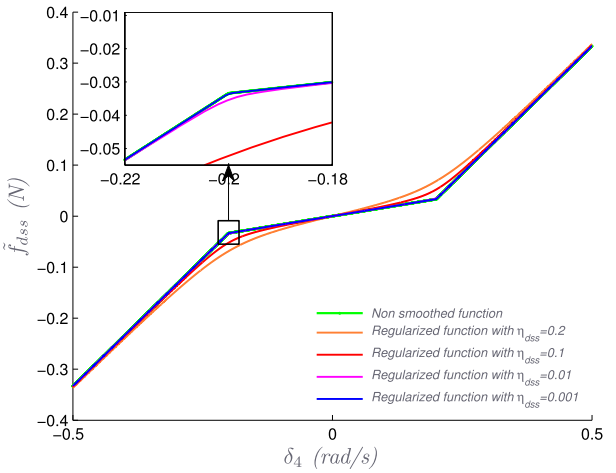

(b) Proposed regularization techniques for the values $\eta_{\mathrm{dss}} = 0.2, 0.1, 0.01, 0.001$.

Fig. 2. Effect of the smoothing parameter σ_{dss} and of the regularization parameter η_{dss} on the abruptness of transition of the approximated function of two-stage stiffness.

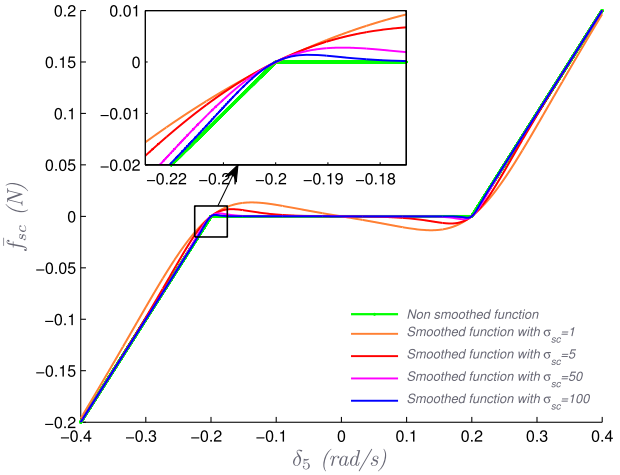

(a) Smoothing technique for the values $\sigma_{\mathrm{sc}} = 1, 5, 50, 100$.

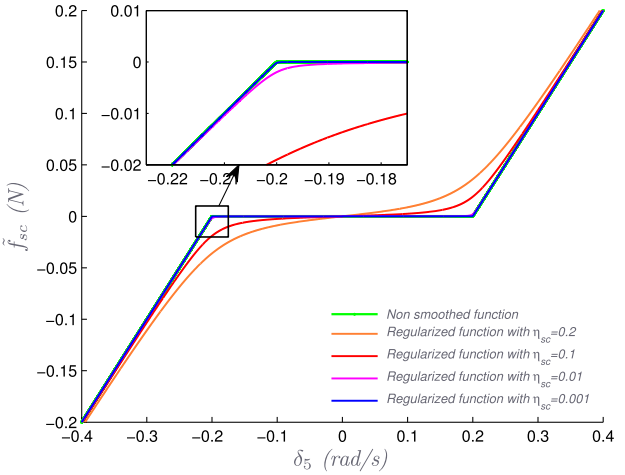

(b) Proposed regularization technique for the values $\eta_{\mathrm{sc}} = 0.2, 0.1, 0.01, 0.001$.

Fig. 3. Effect of the smoothing parameter σ_{sc} and of the regularization parameter η_{sc} on the abruptness of transition of the approximated function of splined clearance.

$$\begin{cases} h_{\mathrm{sc}}(\delta_5) = \sqrt{(\delta_5 - b_{\mathrm{sc}})^2 + 4\eta_{\mathrm{sc}}^2 b_{\mathrm{sc}}^2} \\ g_{\mathrm{sc}}(\delta_5) = \sqrt{(\delta_5 + b_{\mathrm{sc}})^2 + 4\eta_{\mathrm{sc}}^2 b_{\mathrm{sc}}^2} \end{cases} \tag{17}$$

and η_{sc} is the regularization parameter. In Fig. 3, we present a comparison between the proposed regularization and the law obtained by smoothing [11] using the hyperbolic tangent function, which is given by:

$$\bar{f}_{\mathrm{sc}}(\delta_5) = \delta_5 + \frac{1}{2}\left((\delta_5 - b_{\mathrm{sc}})\tanh(\sigma_{\mathrm{sc}}(\delta_5 - b_{\mathrm{sc}})) - (\delta_5 + b_{\mathrm{sc}})\tanh(\sigma_{\mathrm{sc}}(\delta_5 + b_{\mathrm{sc}}))\right) \tag{18}$$

where σ_{sc} is the smoothing parameter. Here we retain the same comments as before.

Similarly, we present below the various regularized laws of torque and forces of friction that are represented by Coulomb's law. The graph of the classical Coulomb model (10) of equation (9) is an irregular function, because it has singularities at the point $\dot{\delta}_i = 0$. The smoothed form [6,8,25] of the torsional friction torque is:

$$\bar{T}_{\mathrm{f}}(\dot{\delta}_i) = T_{\mathrm{s}}\tanh(\sigma_i\dot{\delta}_i), \quad i = 2, 3 \tag{19}$$

Here, we propose as a regularization of the classical model (10), the following function:

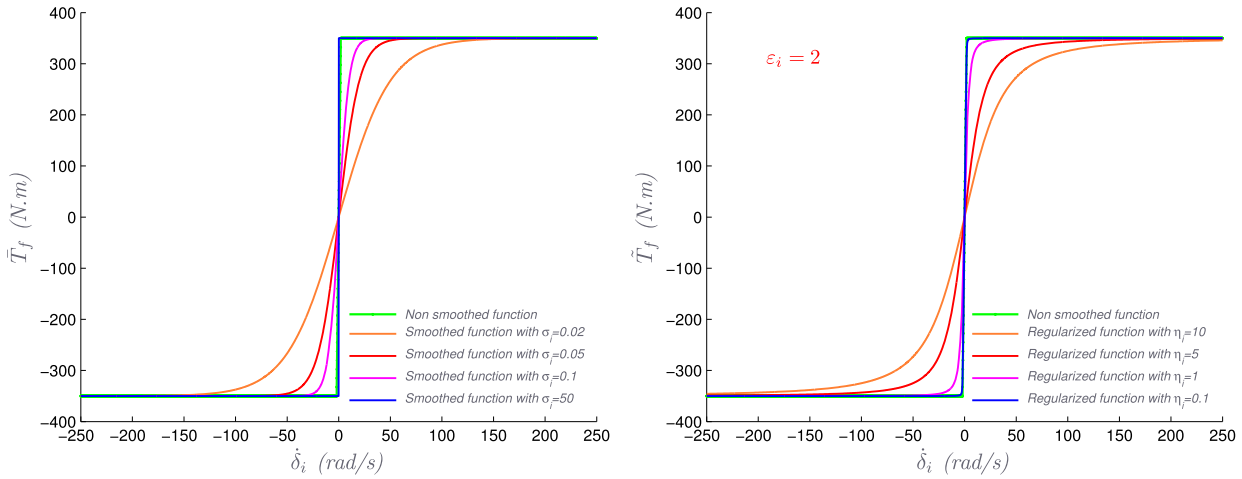

(a) Smoothing technique for the values $\sigma_i = 0.02, 0.05, 0.1, 50$.

(b) Proposed regularization techniques for the values $\eta_i = 10, 5, 1, 0.1$.

Fig. 4. Effect of the smoothing parameter σ_i and of the regularization parameter η_i on the abruptness of the transition of the approximated function of torsional frictions.

$$\tilde{T}_f(\dot{\delta}_i) = \frac{1}{2}\left(h_i(\delta_i) - g_i(\delta_i)\right) \tag{20}$$

where $h_i(\delta_i)$ and $g_i(\delta_i)$ are given by:

$$\begin{cases} h_i(\delta_i) = \sqrt{\left(\frac{T_s}{\varepsilon_i}\right)^2 \left(\varepsilon_i + \dot{\delta}_i\right)^2 + 4\eta_i^2 T_s^2} \\ g_i(\delta_i) = \sqrt{\left(\frac{T_s}{\varepsilon_i}\right)^2 \left(\varepsilon_i - \dot{\delta}_i\right)^2 + 4\eta_i^2 T_s^2} \end{cases} , \quad i = 2, 3 \tag{21}$$

and η_i, $(i = 2, 3)$ are the regularization parameters. Fig. 4 shows that the two studied techniques allow one to have a good approximation.

The function modeling the tangential friction, which is given by the equation (10), is approximated, here, as that of the Coulomb model, by:

$$\begin{cases} \tilde{F}_{T_{x_{1/2}}}(\dot{\delta}_{T_x}) = -\mu_k P \tanh(\sigma_x \dot{\delta}_{T_x}) \\ \tilde{F}_{T_{y_{1/2}}}(\dot{\delta}_{T_y}) = -\mu_k P \tanh(\sigma_y \dot{\delta}_{T_y}) \end{cases} \tag{22}$$

The regularized functions corresponding to those of the equation (10) are given by:

$$\begin{cases} \tilde{F}_{T_{x_{1/2}}}(\dot{\delta}_{T_x}) = -\frac{\mu_k P}{2}(h_{T_x}(\dot{\delta}_{T_x}) - g_{T_x}(\dot{\delta}_{T_x})) \\ \tilde{F}_{T_{y_{1/2}}}(\dot{\delta}_{T_y}) = -\frac{\mu_k P}{2}(h_{T_y}(\dot{\delta}_{T_y}) - g_{T_y}(\dot{\delta}_{T_y})) \end{cases} \tag{23}$$

where $h_{T_x}(\dot{\delta}_{T_x})$, $g_{T_x}(\dot{\delta}_{T_x})$, $h_{T_y}(\dot{\delta}_{T_y})$ and $g_{T_y}(\dot{\delta}_{T_y})$ are expressed by:

$$\begin{cases} h_{T_x}(\dot{\delta}_{T_x}) = \sqrt{(\frac{1}{\varepsilon_x})^2(\varepsilon_x + \dot{\delta}_{T_x})^2 + 4\eta_x^2} \\ g_{T_x}(\dot{\delta}_{T_x}) = \sqrt{(\frac{1}{\varepsilon_x})^2(\varepsilon_x - \dot{\delta}_{T_x})^2 + 4\eta_x^2} \\ h_{T_y}(\dot{\delta}_{T_y}) = \sqrt{(\frac{1}{\varepsilon_x})^2(\varepsilon_y + \dot{\delta}_{T_y})^2 + 4\eta_y^2} \\ g_{T_y}(\dot{\delta}_{T_y}) = \sqrt{(\frac{1}{\varepsilon_x})^2(\varepsilon_y - \dot{\delta}_{T_y})^2 + 4\eta_y^2} \end{cases} \tag{24}$$

Fig. 5 shows the influence of the different parameters that determine the two regularization techniques on the quality of the approximation of the tangential friction action according to the x direction. According to the figures presented above, we note that the value of the regularization parameter that provides good adjustment depends on the shape of the curve of the standard model in the vicinity of singularity points; for example, $\eta_x = 0.1$ for the regularization given in Fig. 5b and $\eta_{dss} = 0.001$ for the regularization given in Fig. 2b. Referring to Figs. 2, 3, 4 and 5, we remark that the proposed

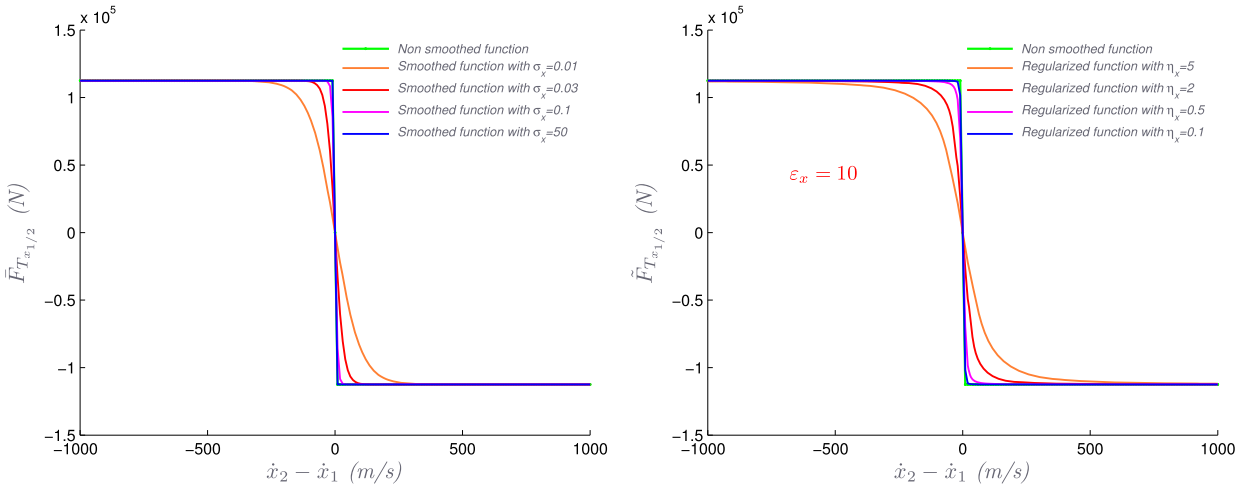

(a) Smoothing technique for the values $\sigma_x = 0.01, 0.03, 0.1, 50$

(b) Proposed regularization techniques for the values $\eta_x = 5, 2, 0.5, 0.1$.

Fig. 5. Effect of the smoothing parameter σ_x and of the regularization parameter η_x on the abruptness of transition of the approximated function of tangential frictions.

regularization gives a better approximation than when replacing by the hyperbolic tangent functions, especially near the singular points.

5. Description of the used algorithm

This section explains the different steps of the algorithm used to solve the nonlinear equation (1) governing the movement of the clutch system via the discrete model. The aim is to use a more realistic approximation of the different contact actions through our regularization and thereafter reducing the computation time expressed here in terms of number of inversions of the tangent matrix compared to incremental iterative methods integrating the regularization of the various contact actions. This technique of regularization allows us, first, to search the solution to the considered problem in the form of a Taylor series expansion and, secondly, to ameliorate the solution to the problem in the vicinity of the singularity zone. The algorithm used is based on the following stages.

5.1. Time discretization

In our modeling, we use the time scheme of Newmark [32] to express the velocity and acceleration vectors at time $t_{n+1} = t_n + \Delta t$ as follows:

$$\begin{cases} \{\ddot{q}^{n+1}\} = a_0(\{q^{n+1}\} - \{q^n\}) - \{\omega^n\} \\ \{\dot{q}^{n+1}\} = \Delta t \beta a_0(\{q^{n+1}\} - \{q^n\}) + \{\psi^n\} \end{cases} \tag{25}$$

where the vectors $\{\omega^n\}$ and $\{\psi^n\}$ are defined by:

$$\begin{aligned} \{\omega^n\} &= a_1\{\dot{q}^n\} + a_2\{\ddot{q}^n\} \\ \{\psi^n\} &= (1 - a_1\Delta t\beta)\{\dot{q}^n\} + (\Delta t(1-\beta) - a_2\Delta t\beta)\{\ddot{q}^n\} \end{aligned} \tag{26}$$

with $a_0 = \frac{1}{\Delta t^2 \gamma}$, $a_1 = \frac{1}{\Delta t \gamma}$, $a_2 = \frac{1}{2\gamma} - 1$, Δt is the time step, the values of coefficients β and γ that ensure the stability of the temporal scheme are given by $\beta = 0.5$ and $\gamma = 0.25$. Taking into account equation (25), the equation of motion (1) written at time t_{n+1} becomes:

$$\begin{aligned} [K_L](\{q^{n+1}\} - \{q^n\}) + f_{sc}^{n+1}\{\varphi_{sc}\} + f_{dss}^{n+1}\{\varphi_{dss}\} + T_f^{n+1}\{\varphi_2\} + T_f^{n+1}\{\varphi_3\} \\ + F_{T_{x_{1/2}}}^{n+1}\{\varphi_{T_x}\} + F_{T_{y_{1/2}}}^{n+1}\{\varphi_{T_y}\} = \{F^{n+1}\} \end{aligned} \tag{27}$$

where $[K_L] = a_0[M] + \Delta t\beta a_0[C] + [K]$, $\{F^{n+1}\} = \{F_{ext}^{n+1}\} + [M]\{\omega^n\} - [C]\{\psi^n\} - [K]\{q^n\}$ and $\{q^{n+1}\}$ is the unknown vector at time t_{n+1}. The different linearization approaches defined with respect to the previous time $t_n = n\Delta t$ which are used in our algorithm are presented in the following condensed form:

$$\{\Delta U\} = \{u^{n+1}\} - \{u^n\} \tag{28}$$

where the vector $\{u^{n+1}\}$ at time t_{n+1} and the increment vector $\{\Delta U\}$ are given by:

$$\begin{cases} {}^{\mathrm{t}}\{u^{n+1}\} = < \{q^{n+1}\}, \delta_{\mathrm{dss}}^{n+1}, h_{\mathrm{dss}}^{n+1}, g_{\mathrm{dss}}^{n+1}, \delta_{\mathrm{sc}}^{n+1}, h_{\mathrm{sc}}^{n+1}, g_{\mathrm{sc}}^{n+1}, \dot{\delta}_2^{n+1}, h_2^{n+1}, g_2^{n+1}, \\ \qquad \dot{\delta}_3^{n+1}, h_3^{n+1}, g_3^{n+1}, \dot{\delta}_{T_x}^{n+1}, h_{T_x}^{n+1}, g_{T_x}^{n+1}, \dot{\delta}_{T_y}^{n+1}, h_{T_y}^{n+1}, g_{T_y}^{n+1} > \\ {}^{\mathrm{t}}\{\Delta U\} = < \{\Delta Q\}, \Delta D_{\mathrm{dss}}, \Delta H_{\mathrm{dss}}, \Delta G_{\mathrm{dss}}, \Delta D_{\mathrm{sc}}, \Delta H_{\mathrm{sc}}, \Delta G_{\mathrm{sc}}, \Delta \dot{D}_2, \Delta H_2, \\ \qquad \Delta G_2, \Delta \dot{D}_3, \Delta H_3, \Delta G_3, \Delta \dot{D}_{T_x}, \Delta H_{T_x}, \Delta G_{T_x}, \Delta \dot{D}_{T_y}, \Delta H_{T_y}, \Delta G_{T_y} > \end{cases} \tag{29}$$

Taking into account equation (28), the problem (27) discretized in time verified by new incremental unknowns is written in the following reduced form:

$$[K_T^n]\{\Delta Q\} + \{F(\{\Delta Q\}, \{\Delta Q\})\} = \{S^{n+1}\} \tag{30}$$

where $[K_T^n]$ is the tangent matrix evaluated at time t_n given by:

$$\begin{aligned} [K_T^n] = {} & a_0[M] + \Delta t \beta a_0 [C] + [K] + [K_{T_{\mathrm{dss}}}^n] + [K_{T_{\mathrm{sc}}}^n] + [K_{T_{x_{1/2}}}^n] \\ & + [K_{T_{y_{1/2}}}^n] + [K_{T_2}^n] + [K_{T_3}^n] \end{aligned} \tag{31}$$

with

$$\begin{cases} [K_{T_{\mathrm{dss}}}^n] = (1 + \frac{(1-\alpha_{\mathrm{dss}})^2}{2}(\frac{(\delta_{\mathrm{dss}}^n - b_{\mathrm{dss}})}{h_{\mathrm{dss}}^n} - \frac{(\delta_{\mathrm{dss}}^n + b_{\mathrm{dss}})}{g_{\mathrm{dss}}^n}))\{\varphi_{\mathrm{dss}}\} < \chi_{\mathrm{dss}} > \\ [K_{T_{\mathrm{sc}}}^n] = (1 + \frac{1}{2}(\frac{(\delta_{\mathrm{sc}}^n - b_{\mathrm{sc}})}{h_{\mathrm{sc}}^n} - \frac{(\delta_{\mathrm{sc}}^n + b_{\mathrm{sc}})}{g_{\mathrm{sc}}^n}))\{\varphi_{\mathrm{sc}}\} < \chi_{\mathrm{sc}} > \\ [K_{T_2}^n] = \frac{1}{2}(\frac{(\frac{T_s}{\xi})^2(\xi + \dot{\delta}_2^n)}{h_2^n} + \frac{(\frac{T_s}{\xi})^2(\xi - \dot{\delta}_2^n)}{g_2^n})\Delta t \beta a_0 \{\varphi_2\} < \chi_2 > \\ [K_{T_3}^n] = \frac{1}{2}(\frac{(\frac{T_s}{\xi})^2(\xi + \dot{\delta}_3^n)}{h_3^n} + \frac{(\frac{T_s}{\xi})^2(\xi - \dot{\delta}_3^n)}{g_3^n})\Delta t \beta a_0 \{\varphi_3\} < \chi_3 > \\ [K_{T_{x_{1/2}}}^n] = -\frac{\mu_k P}{2}(\frac{(\frac{1}{\varrho})^2(\varrho + \dot{\delta}_{T_x}^n)}{h_{T_x}^n} + \frac{(\frac{1}{\varrho})^2(\varrho - \dot{\delta}_{T_x}^n)}{g_{T_x}^n})\Delta t \beta a_0 \{\varphi_{T_x}\}(< \nu_{x_2} > - < \nu_{x_1} >) \\ [K_{T_{y_{1/2}}}^n] = -\frac{\mu_k P}{2}(\frac{(\frac{1}{\varrho})^2(\varrho + \dot{\delta}_{T_y}^n)}{h_{T_y}^n} + \frac{(\frac{1}{\varrho})^2(\varrho - \dot{\delta}_{T_y}^n)}{g_{T_y}^n})\Delta t \beta a_0 \{\varphi_{T_y}\}(< \nu_{y_2} > - < \nu_{y_1} >) \end{cases} \tag{32}$$

the quadratic form $\{F(\{\Delta Q\}, \{\Delta Q\})\}$ is defined by:

$$\begin{aligned} \{F(\{\Delta Q\}, \{\Delta Q\})\} = {} & \{F_{\mathrm{dss}}(\{\Delta Q\}, \{\Delta Q\})\} + \{F_{\mathrm{sc}}(\{\Delta Q\}, \{\Delta Q\})\} \\ & + \{F_2(\{\Delta Q\}, \{\Delta Q\})\} + \{F_3(\{\Delta Q\}, \{\Delta Q\})\} \\ & + \{F_{T_{x_{1/2}}}(\{\Delta Q\}, \{\Delta Q\})\} + \{F_{T_{y_{1/2}}}(\{\Delta Q\}, \{\Delta Q\})\} \end{aligned} \tag{33}$$

with

$$\begin{cases} \{F_{\mathrm{dss}}(\{\Delta Q\}, \{\Delta Q\})\} = \frac{1}{4}((1-\alpha_{\mathrm{dss}})^2(\frac{1}{h_{\mathrm{dss}}^n} - \frac{1}{g_{\mathrm{dss}}^n})\Delta D_{\mathrm{dss}}^2 - \frac{\Delta H_{\mathrm{dss}}^2}{h_{\mathrm{dss}}^n} + \frac{\Delta G_{\mathrm{dss}}^2}{g_{\mathrm{dss}}^n})\{\varphi_{\mathrm{dss}}\} \\ \{F_{\mathrm{sc}}(\{\Delta Q\}, \{\Delta Q\})\} = \frac{1}{4}((\frac{1}{h_{\mathrm{sc}}^n} - \frac{1}{g_{\mathrm{sc}}^n})\Delta D_{\mathrm{sc}}^2 - \frac{\Delta H_{\mathrm{sc}}^2}{h_{\mathrm{sc}}^n} + \frac{\Delta G_{\mathrm{sc}}^2}{g_{\mathrm{sc}}^n})\{\varphi_{\mathrm{sc}}\} \\ \{F_2(\{\Delta Q\}, \{\Delta Q\})\} = \frac{1}{4}((\frac{T_s}{\xi})^2(\frac{1}{h_2^n} - \frac{1}{g_2^n})\Delta \dot{D}_2^2 - \frac{\Delta H_2^2}{h_2^n} + \frac{\Delta G_2^2}{g_2^n})\{\varphi_2\} \\ \{F_3(\{\Delta Q\}, \{\Delta Q\})\} = \frac{1}{4}((\frac{T_s}{\xi})^2(\frac{1}{h_3^n} - \frac{1}{g_3^n})\Delta \dot{D}_3^2 - \frac{\Delta H_3^2}{h_3^n} + \frac{\Delta G_3^2}{g_3^n})\{\varphi_3\} \\ \{F_{T_{x_{1/2}}}(\{\Delta Q\}, \{\Delta Q\})\} = -\frac{\mu_k P}{4}((\frac{1}{\varrho})^2(\frac{1}{h_{T_x}^n} - \frac{1}{g_{T_x}^n})\Delta \dot{D}_{T_x}^2 - \frac{\Delta H_{T_x}^2}{h_{T_x}^n} + \frac{\Delta G_{T_x}^2}{g_{T_x}^n})\{\varphi_{T_x}\} \\ \{F_{T_{y_{1/2}}}(\{\Delta Q\}, \{\Delta Q\})\} = -\frac{\mu_k P}{4}((\frac{1}{\varrho})^2(\frac{1}{h_{T_y}^n} - \frac{1}{g_{T_y}^n})\Delta \dot{D}_{T_y}^2 - \frac{\Delta H_{T_y}^2}{h_{T_y}^n} + \frac{\Delta G_{T_y}^2}{g_{T_y}^n})\{\varphi_{T_y}\} \end{cases} \tag{34}$$

and the right-hand side $\{S^{n+1}\}$, which depends on the solution at time $t_n = n\Delta t$, is given by:

$$\{S^{n+1}\} = \{F^{n+1}\} - \{S_{\mathrm{dss}}^n\} - \{S_{\mathrm{sc}}^n\} - \{S_2^n\} - \{S_3^n\} - \{S_{T_{x_{1/2}}}^n\} - \{S_{T_{y_{1/2}}}^n\} \tag{35}$$

with

$$\begin{cases} \{F^{n+1}\} &= \{F_{\text{ext}}^{n+1}\} + [M]\{\omega^n\} - [C]\{\psi^n\} - [K]\{q^n\} \\ \{S_{\text{dss}}^n\} &= f_{\text{dss}}(\delta_{\text{dss}}^n)\{\varphi_{\text{dss}}\} \\ \{S_{\text{sc}}^n\} &= f_{\text{sc}}(\delta_{\text{sc}}^n)\{\varphi_{\text{sc}}\} \\ \{S_2^n\} &= T_f(\dot{\delta}_2^n)\{\varphi_2\} + \frac{1}{2}\left(\frac{(\frac{T_s}{\xi})^2(\xi+\dot{\delta}_2^n)}{h_2^n} + \frac{(\frac{T_s}{\xi})^2(\xi-\dot{\delta}_2^n)}{g_2^n}\right)(-\dot{\delta}_2^n + < \chi_2 > \{\psi^n\})\{\varphi_2\} \\ \{S_3^n\} &= T_f(\dot{\delta}_3^n)\{\varphi_3\} + \frac{1}{2}\left(\frac{(\frac{T_s}{\xi})^2(\xi+\dot{\delta}_3^n)}{h_3^n} + \frac{(\frac{T_s}{\xi})^2(\xi-\dot{\delta}_3^n)}{g_3^n}\right)(-\dot{\delta}_3^n + < \chi_3 > \{\psi^n\})\{\varphi_3\} \\ \{S_{T_{x_{1/2}}}^n\} &= F_{T_{x_{1/2}}}^n\{\varphi_{T_x}\} - \frac{\mu_k P}{2}\left(\frac{(\frac{1}{\varrho})^2(\varrho+\dot{\delta}_{T_x}^n)}{h_{T_x}^n} + \frac{(\frac{1}{\varrho})^2(\varrho-\dot{\delta}_{T_x}^n)}{g_{T_x}^n}\right)(-\dot{x}_2^n + \dot{x}_1^n \\ &\quad + (< \nu_{x_2} > - < \nu_{x_1} >)\{\psi^n\})\{\varphi_{T_x}\} \\ \{S_{T_{y_{1/2}}}^n\} &= F_{T_{y_{1/2}}}^n\{\varphi_{T_y}\} - \frac{\mu_k P}{2}\left(\frac{(\frac{1}{\varrho})^2(\varrho+\dot{\delta}_{T_y}^n)}{h_{T_y}^n} + \frac{(\frac{1}{\varrho})^2(\varrho-\dot{\delta}_{T_y}^n)}{g_{T_y}^n}\right)(-\dot{y}_2^n + \dot{y}_1^n \\ &\quad + (< \nu_{y_2} > - < \nu_{y_1} >)\{\psi^n\})\{\varphi_{T_y}\} \end{cases} \tag{36}$$

5.2. Homotopy transformation

In order to apply the perturbation technique, we transform, firstly, problem (30) into an artificial problem obtained by homotopy transformation [16,20,33]. The homotopy transformation used here consists in introducing, on the one hand, a perturbation parameter ϵ, and, on the other hand, an arbitrary invertible matrix $[K^*]$ as follows:

$$[K^*]\{\Delta W\} + \epsilon([K_T^n] - [K^*])\{\Delta W\} + \epsilon\{F(\{\Delta W\}, \{\Delta W\})\} = \{S^{n+1}\} \tag{37}$$

where $\{\Delta W(\epsilon)\}$ is the new unknown vector of the artificial problem (37), which depends on the perturbation parameter ϵ in such a way that, for $\epsilon = 0$, we obtain a problem simple to solve, and, for $\epsilon = 1$, we obtain the solution to problem (30).

5.3. Series expansion and continuation procedure

The solution to the artificial problem (37) is sought in the series expansion form [34,35] truncated at order p with respect to a perturbation parameter ϵ as follows:

$$\{\Delta W\} = \{\Delta W_0\} + \sum_{k=1}^{p} \epsilon^k \{\Delta W_k\} \tag{38}$$

The validity range of this series expansion is defined by the criterion [18,20,35,36] given by:

$$\epsilon_{\max} = \left(\kappa \frac{\|\{\Delta W_1\}\|}{\|\{\Delta W_p\}\|}\right)^{\frac{1}{p-1}} \tag{39}$$

where κ is a given tolerance parameter. Taking into account the series expansion (38), the problem (37) is transformed into a succession of linear problems of the same tangent matrix $[K^*]$ as:

$$\begin{aligned} &Order \quad 0 \qquad\quad : \quad [K^*]\{\Delta W_0\} = \{S^{n+1}\} \\ &Order \quad 1 \le k \le p \quad : \quad [K^*]\{\Delta W_k\} = -([K_T^n] - [K^*])\{\Delta W_{k-1}\} \\ &\qquad\qquad\qquad\qquad\qquad\quad - \textstyle\sum_{r=0}^{k-1}\{FQ(\{\Delta W_r\}, \{\Delta W_{k-1-r}\})\} \end{aligned} \tag{40}$$

If $(\epsilon_{\max} \ge 1)$ then the solution to the initial problem (30) at time t_{n+1} is given by:

$$\{q^{n+1}\} = \{q^n\} + \{\Delta W(\epsilon = 1)\} \tag{41}$$

If $(\epsilon_{\max} < 1)$, the continuation process functions with a matrix $[K^*] = [K_T^n]$ evaluated as the starting solution to each step to build a new branch solution. Let us note that the computation of each branch solution is achieved using a single inversion of the arbitrary matrix $[K^*]$.

Table 1
Parameters used for simulating the studied clutch system.

Parameters and excitation	Values
Torsional inertias (kg·m^2)	$I_1 = 0.2$, $I_2 = 12{\cdot}10^{-3}$, $I_3 = 83{\cdot}10^{-4}$, $I_4 = 2{\cdot}10^{-4}$, $I_5 = 18{\cdot}10^{-2}$
Masses (kg)	$m_1 = 10$, $m_2 = 1.17$, $m_3 = 0.8$, $m_4 = 0.2$, $m_5 = 9$
Torsional damping (N·m·rad/s)	$c_{34} = 0.1$, $c_{45} = 0.1$
Linear damping (N·s/m)	$c_{x_i} = c_{y_i} = c_{z_i} = 0.1$ $(i = 1, 2)$
Bearing stiffness (N/m)	$k_{x_i} = k_{y_i} = k_{z_i} = 10^{10}$ $(i = 1, 2)$
Torsional spring stiffness (N·m/rad)	$k_d = 8{\cdot}10^5$, $K_{dss} = 17500$, $K_{sc} = 3{\cdot}10^5$
Saturation friction torque (N·m)	$T_s = 350$
Torque excitation amplitude (N·m)	$T_m = 300$, $T_p = 250$
Excitation frequency (Hz)	$F_e = 30$
Receiving torque (N·m)	$T_D = T_m$
The static friction coefficient	$\mu_s = 0.3$
The kinetic friction coefficient	$\mu_k = 0.75\,\mu_s$
	$P = 5{\cdot}10^5$ N/m^2, $b_{sc} = 0.2$ rad, $b_{dss} = 0.125$ rad, $\alpha_{dss} = 0.167$

6. Results and discussions

To demonstrate the efficiency and effectiveness of the used approach to simulate the nonlinear dynamic response of a clutch mechanism, we take the same application as that made in the work of Driss et al. [15] with the same data as that listed in Table 1. The values of the time step and those of the coefficients used in the time scheme Newmark are: $\Delta t = 4{\cdot}10^{-7}$ s, $\gamma = 0.25$ and $\beta = 0.5$. To define the optimal regularization parameters, we have opted for a numerical experimentation with the used algorithm and the Newton–Raphson method. In a first time, we will carry out a numerical study with the Newton–Raphson method while comparing the two approximation types for the considered contact: the proposed regularization operations and smoothed functions (hyperbolic tangent). In a second time, the same numerical study will be done with the used algorithm to reduce computation time. This study will be our objective in the following paragraphs.

6.1. Numerical study with Newton–Raphson method

In order to determine the optimum values of the regularization parameters, which allow us to have a good approximation, a preliminary numerical experimentation has been performed. According to this numerical experimentation, the optimum values of these parameters are: $\eta_x = \eta_y = 10^{-2}$, $\eta_{sc} = \eta_{dss} = 10^{-4}$, $\eta_2 = \eta_3 = 10^{-3}$, $\epsilon_x = \epsilon_y = 8$, $\epsilon_2 = 0.08$, $\epsilon_3 = 0.008$. Regarding the smoothing parameters, we adopted those used in reference [8]: $\sigma_x = \sigma_y = 50$, $\sigma_{sc} = \sigma_{dss} = 100$, $\sigma_2 = \sigma_3 = 50$. The tolerance parameter used in the Newton–Raphson method is fixed at $\kappa = 10^{-4}$. In this section, we will use the Newton–Raphson method to compare the two types of approximations: smoothing functions and regularized functions. This study is the subject of the first original idea for this article: Comparison between the tangent hyperbolic and the proposed regularizations by using the Newton–Raphson Method. In the following, the solution will be searched for so that the residue is less than 10^{-4}.

In Fig. 6, we represent the relative angular displacements δ_4 and δ_5 with respect to time in the cases of smoothed and regularized functions. From this figure, we can see that there is a difference between the curves using the regularized functions and those using smoothing functions. This difference shows that smoothing functions do not represent well the discontinuity conditions (see Fig. 7). The obtained solutions require 595391 inversions of tangent matrix for the regularized functions and 605054 inversions of tangent matrix for the smoothing function. In Fig. 6e, we notice that the duration of the contact loss is greater in the case of the regularized functions that in the case of smoothing functions. To reduce the computation time, we will use the high-order algorithm detailed above in the following paragraph for the regularized functions only.

6.2. Numerical study with the used algorithm

In this section, we will discuss and compare the used algorithm and the Newton–Raphson method in the case of regularized functions. The solution's quality will be examined by computing the residue of equation (1). The used algorithm is applied to simulate the problem of equation (1) with the same values of the regularization parameters as those that were used in the previous section. In the following, we will study the influence of the truncation order on the number of length steps required to compute the solution on the considered time interval by fixing the tolerance parameter $\kappa = 10^{-9}$. In Table 2, we report the number of steps for truncation orders $p = 12, 13, 14, 16, 20, 25$. From this table, we remark that the used algorithm starts functioning from truncation order $p = 13$ and that the number of steps decreases when the truncation order increases.

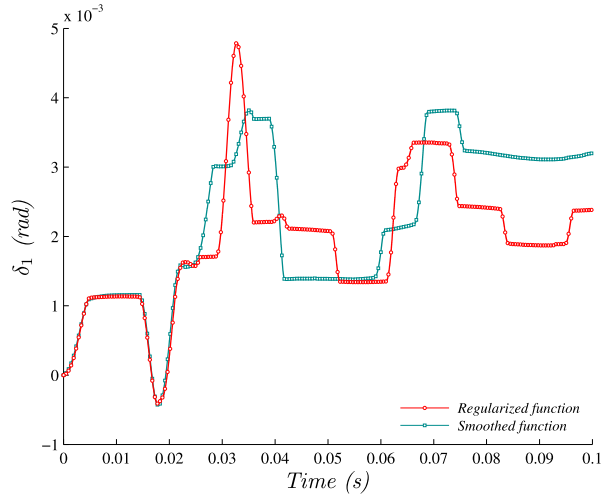

(a) δ_1 versus the time

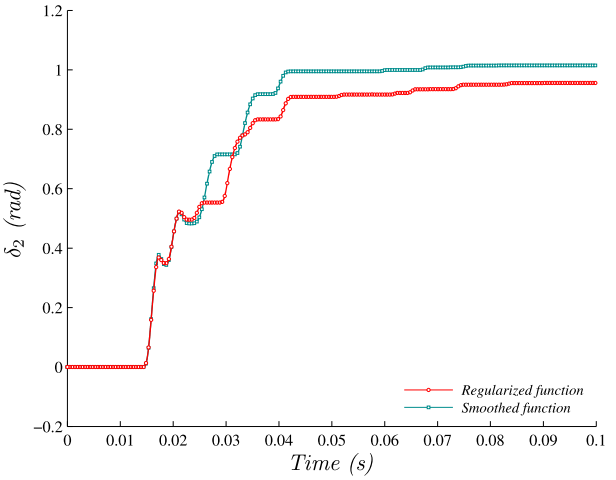

(b) δ_2 versus the time

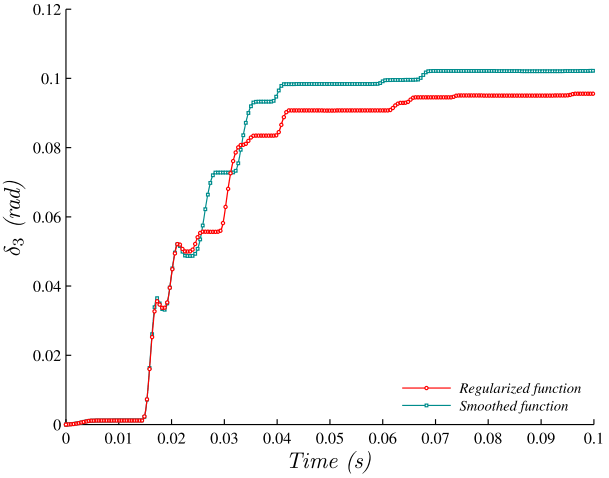

(c) δ_3 versus the time

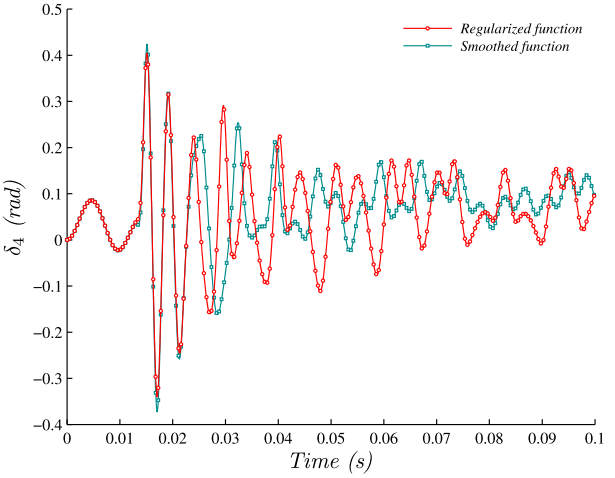

(d) δ_4 versus the time

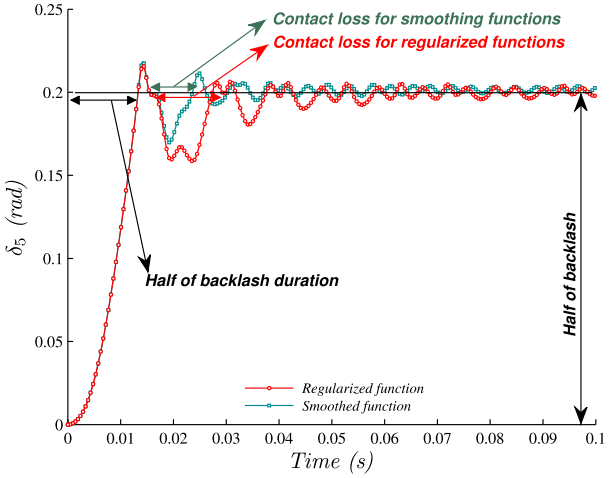

(e) δ_5 versus the time

Fig. 6. Relative angular displacements δ_i, $i = 1 \ldots 5$ with respect to time in the cases of smoothed and regularized functions.

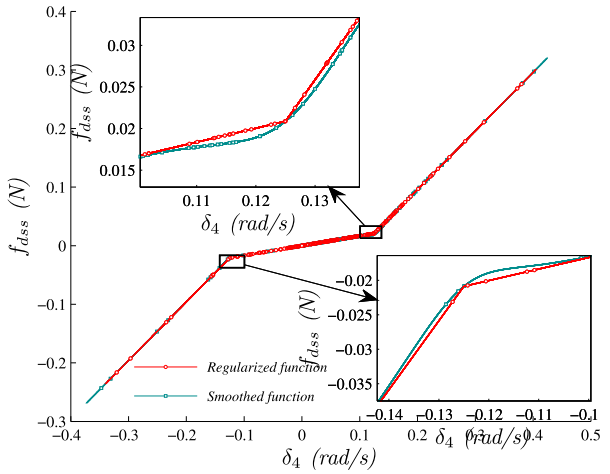

(a) f_{dss} versus the relative angular displacement δ_4.

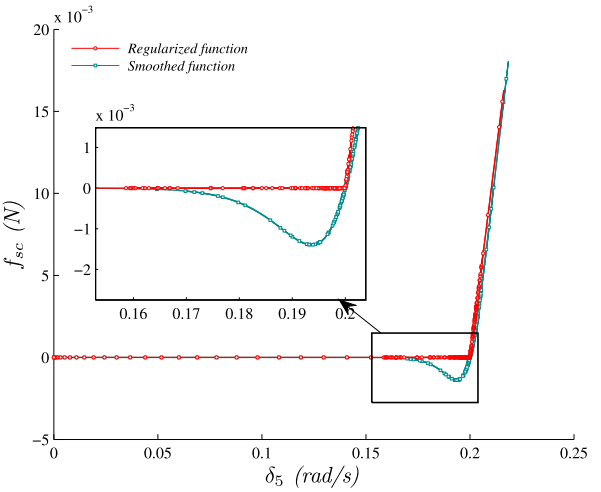

(b) f_{sc} versus the relative angular displacement δ_5.

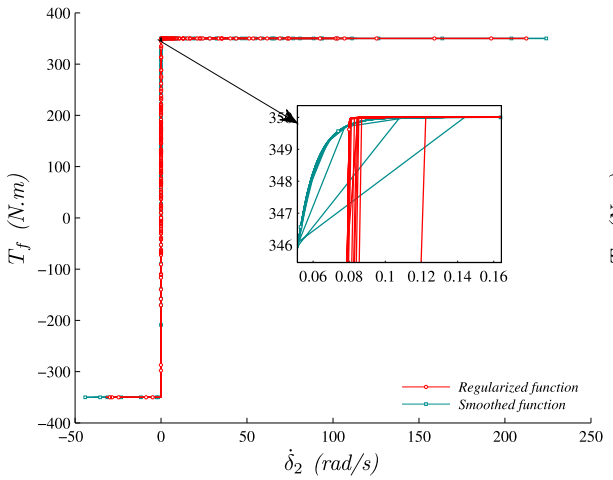

(c) T_f versus the relative angular velocity $\dot{\delta}_2$.

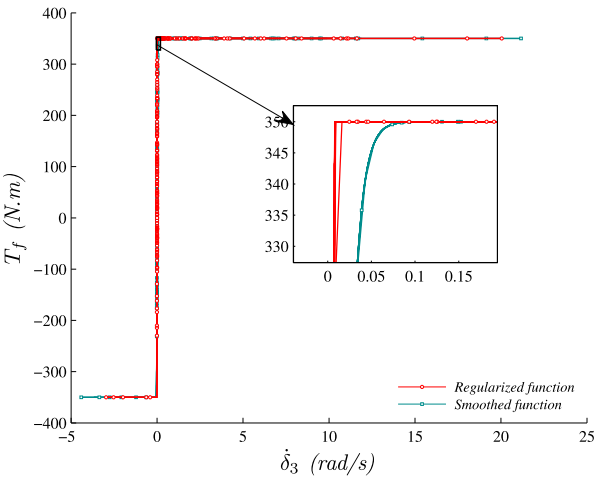

(d) T_f versus the relative angular velocity $\dot{\delta}_3$.

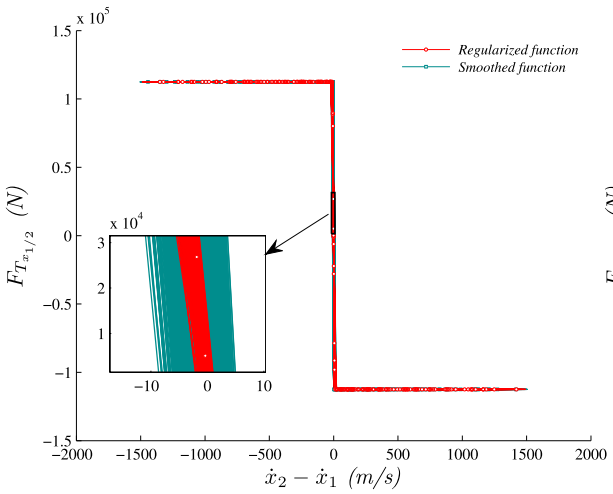

(e) $F_{T_{x_{1/2}}}$ versus the relative velocity $\dot{x}_2 - \dot{x}_1$.

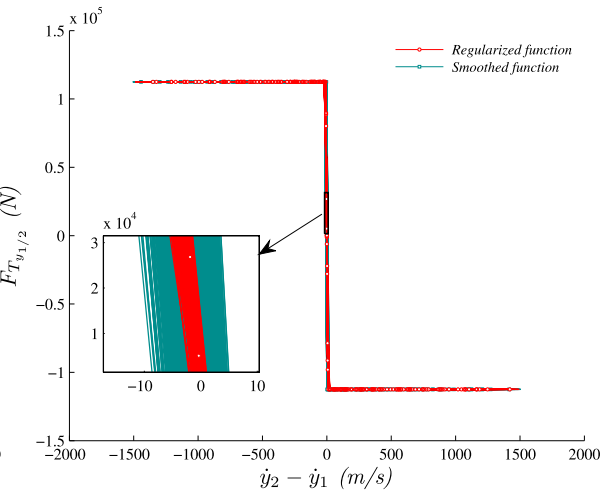

(f) $F_{T_{y_{1/2}}}$ versus the relative velocity $\dot{y}_2 - \dot{y}_1$.

Fig. 7. Different contact actions in the cases of smoothed and regularized functions.

Table 2
Influence of the truncation order on the number of steps for the tolerance parameter $\kappa = 10^{-9}$.

Truncation order	12	13	14	16	20	25
Number of steps	Diverge	546	520	488	441	405

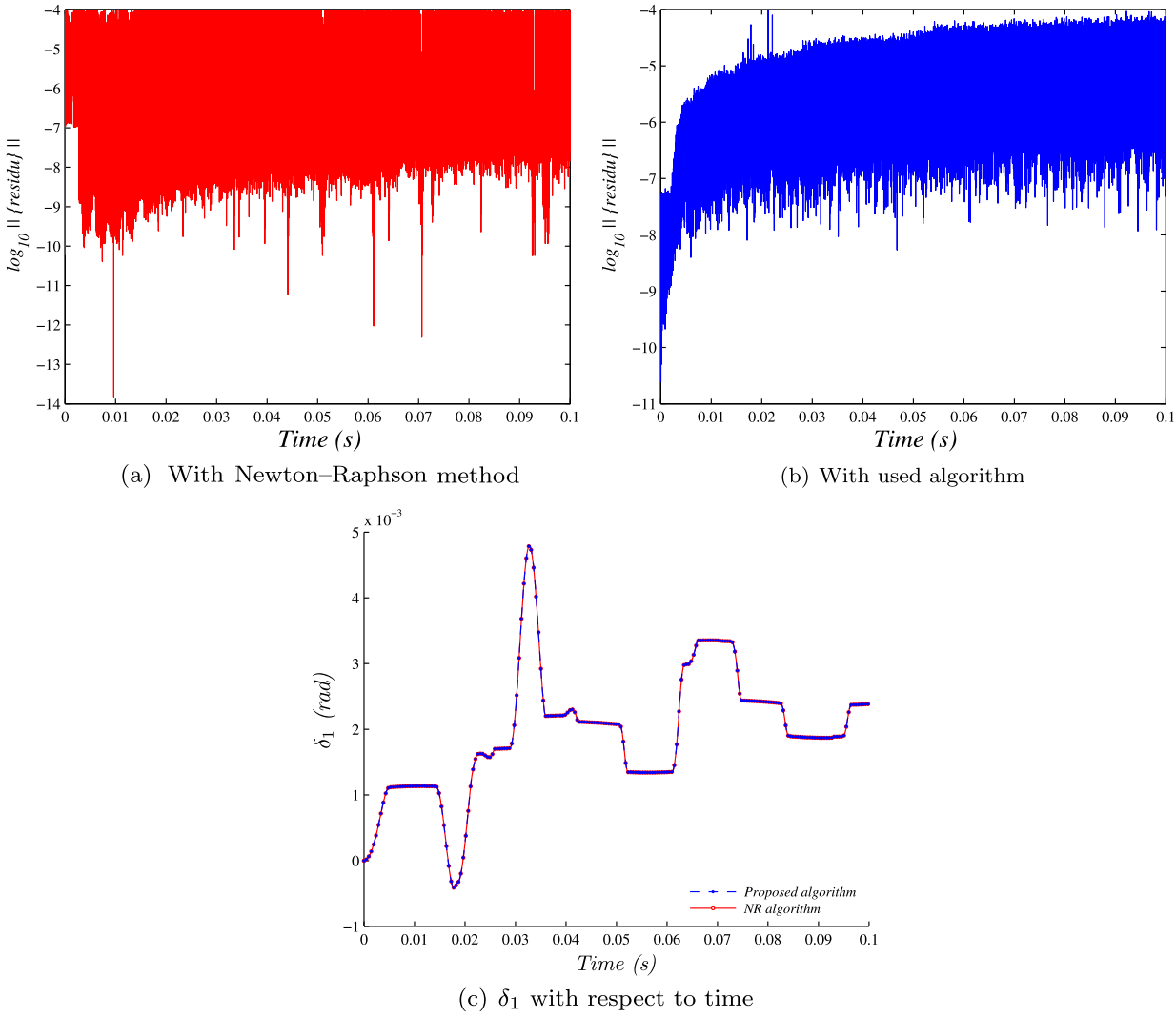

Fig. 8. Decimal logarithm of the residual norm with respect to time for the case of regularized functions and comparison of results obtained by the used algorithm and by the Newton–Raphson method.

Thereafter, we will adopt truncation order $p = 14$ and tolerance parameter $\kappa = 10^{-9}$ for the used algorithm and the tolerance parameter $\kappa = 10^{-4}$ for the Newton–Raphson method. In Fig. 8, we represent the solution quality represented by the decimal logarithm of the residual vector norm versus time. According to this figure, we remark that the solution quality is always less than 10^{-4} so that we can compare the two methods.

In Fig. 8c, we represent the evolution of δ_1 with respect to time for the case of regularized functions obtained by both algorithms. These solution curves require 520 inversions of matrix $[K^*]$ with the used algorithm and 598480 inversions of tangent matrix with the Newton–Raphson method. This comparison confirms the robustness, accuracy, and efficiency of the used algorithm.

7. Conclusion

In this work, we have used a high-order algorithm for simulating the nonlinear dynamic behavior of the clutch system. This algorithm combines the high-order implicit technique based on developments in Taylor series coupled with Newmark's integration scheme in a continuation procedure. The original idea is the proposition of new continuous functions

which approximate the singular functions of the contact actions. The obtained results are convincing compared to the Newton–Raphson method with two types of approximation: smoothing function and regularized functions. The used algorithm requires no correction and one inversion of the iteration matrix allows us to get a good part of the solution. The key points in this high-order implicit algorithm are first a high-order solver based on developments in Taylor series, second the possibility of choosing the tangent matrix $[K^*]$, which limits the number of matrices to be triangulated. Let us recall that the used algorithm solves the nonlinear dynamic behavior of the clutch system with a high-order predictor without any correction. This comparison confirms the robustness, accuracy and efficiency of the used algorithm. Compared to the Newton–Raphson method, the used algorithm is found competitive in terms of computational cost versus accuracy and benefit from a simple implementation. According to the obtained results, the proposed regularized functions have yielded encouraging results.

References

[1] C. Padmanabhan, R. Singh, Dynamics of a piecewise non-linear system subject to dual harmonic excitation using parametric continuation, J. Sound Vib. 184 (5) (1995) 767–799.
[2] C. Gaillard, R. Singh, Dynamic analysis of automotive clutch dampers, Appl. Acoust. 60 (2000) 399–424.
[3] C. Duan, R. Singh, Super-harmonics in a torsional system with dry friction path subject to harmonic excitation under a mean torque, J. Sound Vib. 285 (2005) 803–834.
[4] C. Duan, R. Singh, Transient responses of a 2-dof torsional system with nonlinear dry friction under a harmonically varying normal load, J. Sound Vib. 285 (2005) 1223–1234.
[5] Y. Driss, T. Fakhfakh, M. Haddar, Dynamics of a five degree of freedom torsional system with dry friction path and clearance nonlinearity, Int. Rev. Mech. Eng. 1 (1) (2007) 61–69.
[6] Y. Driss, T. Fakhfakh, M. Haddar, Effect of eccentricity on a clutch system under a harmonically varying normal load, J. Fail. Anal. Prev. 7 (2007) 127–136.
[7] L. Walha, T. Fakhfakh, M. Haddar, Nonlinear dynamics of a two-stage gear system with mesh stiffness fluctuation, bearing flexibility and backlash, Mech. Mach. Theory 44 (5) (2009) 1058–1069.
[8] L. Walha, Y. Driss, M.T. Khabou, T. Fakhfakh, M. Haddar, Effects of eccentricity defect on the nonlinear dynamic behavior of the mechanism clutch-helical two stage gear, Mech. Mach. Theory 46 (7) (2011) 986–997.
[9] J.R. Dormand, P.J. Prince, A family of embedded Runge–Kutta formulae, J. Comput. Appl. Math. 6 (1) (1980) 19–26.
[10] C. Duan, Dynamic analysis of dry friction path in a torsional system, Ph.D. thesis, The Ohio State University, 2004.
[11] L. Walha, T. Fakhfakh, M. Haddar, Backlash effect on dynamic analysis of a two-stage spur gear system, J. Fail. Anal. Prev. 6 (3) (2006) 60–68.
[12] C. Duan, R. Singh, Dynamic analysis of preload nonlinearity in a mechanical oscillator, J. Sound Vib. 301 (3–5) (2007) 963–978.
[13] T.S. Osman, J.T. Dreyer, R. Singh, Order domain analysis of speed-dependent friction-induced torque in a brake experiment, J. Sound Vib. 331 (23) (2012) 5040–5053.
[14] T.C. Kim, T.E. Rook, R. Singh, Effect of smoothening functions on the frequency response of an oscillator with clearance non-linearity, J. Sound Vib. 263 (3) (2003) 665–678.
[15] Y. Driss, T. Fakhfakh, M. Haddar, Dynamics of a five-degree-of-freedom torsional system with dry friction path and clearance nonlinearity, Int. J. Numer. Anal. Methods Eng. 2 (1) (2014) 19–27.
[16] M. Jamal, B. Braikat, S. Boutmir, N. Damil, M. Potier-Ferry, A high order implicit algorithm for solving instationary non-linear problems, Comput. Mech. 28 (5) (2002) 375–380.
[17] B. Braikat, M. Jamal, N. Damil, Algorithmes d'intégration temporelle implicites couplés avec des résoluteurs d'ordre élevé, Rev. Eur. Éléments Finis 11 (6) (2002) 749–772.
[18] S. Boutmir, B. Braikat, M. Jamal, N. Damil, B. Cochelin, M. Potier-Ferry, Des solveurs implicites d'ordre supérieur pour les problèmes de dynamique non linéaire des structures, Rev. Eur. Éléments Finis 13 (5–7) (2004) 449–460.
[19] B. Braikat, M. Jamal, N. Damil, Utilisation des techniques de la méthode asymptotique numérique pour la résolution des problèmes instationnaires non linéaires, Rev. Eur. Éléments Finis 13 (1–2) (2004) 119–139.
[20] A. Timesli, B. Braikat, H. Lahmam, H. Zahrouni, A new algorithm based on moving least square method to simulate material mixing in friction stir welding, Eng. Anal. Bound. Elem. 50 (2015) 372–380.
[21] M.A. Crisfield, Faster modified Newton–Raphson iteration, Comput. Methods Appl. Mech. Eng. 20 (3) (1979) 267–278.
[22] R. Singh, H. Xie, R.J. Comparin, Analysis of Automotive Neutral Gear Rattle, Academic Press Limited, 1989.
[23] T.C. Kim, T.E. Rook, R. Singh, Super and sub-harmonic response calculations for a torsional system with clearance nonlinearity using the harmonic balance method, J. Sound Vib. 281 (3–5) (2005) 965–993.
[24] C. Duan, R. Singh, Dynamics of a 3-dof torsional system with a dry friction controlled path, J. Sound Vib. 289 (4–5) (2006) 657–688.
[25] C. Duan, R. Singh, Forced vibrations of a torsional oscillator with coulomb friction under a periodically varying normal load, J. Sound Vib. 325 (3) (2009) 499–506.
[26] H. Dresig, F. Holzweißig, Dynamics of Machinery: Theory and Applications, Springer-Verlag, Berlin, Heidelberg, 2010.
[27] E.J. Berger, Friction modeling for dynamic system simulation, Appl. Mech. Rev. 55 (6) (2002) 535–577.
[28] C. Duan, R. Singh, Isolated sub-harmonic resonance branch in the frequency response of an oscillator with slight asymmetry in the clearance, J. Sound Vib. 314 (1–2) (2008) 12–18.
[29] M. Potier-Ferry, N. Damil, B. Braikat, J. Descamps, J.-M. Cadou, H.L. Cao, A.E. Hussein, Treatment of strong non-linearities by the asymptotic numerical method, C. R. Acad. Sci., Sér. IIB Mechanics Phys. Chem. Astron. 3 (324) (1997) 171–177.
[30] H. Mottaqui, B. Braikat, N. Damil, Discussion about parameterization in the asymptotic numerical method: application to nonlinear elastic shells, Comput. Methods Appl. Mech. Eng. 199 (2010) 1701–1709.
[31] H. Mottaqui, B. Braikat, N. Damil, Local parameterization and the asymptotic numerical method, Math. Model. Nat. Phenom. 5 (2010) 16–22.
[32] N.M. Newmark, A method of computation for structural dynamics, in: Proceedings of ASCE, vol. 85, 1959.
[33] E.L. Allgower, K. Georg, Numerical Continuation Methods: An Introduction, Springer Series in Computational Mathematics, vol. 13, 1990.
[34] N. Damil, M. Potier-Ferry, A new method to compute perturbed bifurcations: application to the buckling of imperfect elastic structures, Int. J. Eng. Sci. 28 (9) (1990) 943–957.
[35] B. Cochelin, N. Damil, M. Potier-Ferry, Méthode asymptotique numérique, Hermès-Lavoisier, Paris, 2007.
[36] B. Cochelin, A path-following technique via an asymptotic-numerical method, Comput. Struct. 53 (5) (1994) 1181–1192.